Beam polarization asymmetry and the electromagnetic production of kaons from protons

Oren V. Maxwell
Department of Physics, Florida International University, Miami, Florida 33199, USA
(Received 1 November 2012; revised manuscript received 4 December 2012; published 26 December 2012)

The beam polarization asymmetry in the reaction $ep \to e'K^+\Lambda$ has been investigated in a tree-level effective Lagrangian model. The model incorporates most of the well-established baryon resonances with spins up to $\frac{5}{2}$, four less well-established nucleon resonances with larger mass, and the two kaon resonances $K^\star(892)$ and $K1(1270)$. The off-shell structure of the electromagnetic vertices was accounted for by the inclusion of electromagnetic form factors at those vertices. The free parameters of the model were fitted in a previous study to a large pool of photoproduction data from the CLAS, GRAAL, SAPHIR, and LEPS collaborations and to CLAS data for the virtual photoproduction structure functions σ_U, σ_T, σ_L, σ_{TT}, and σ_{LT}. Using this model, results were obtained for the beam polarization asymmetry structure function $\sigma_{LT'}$ and compared with CLAS data. Two new fits to the combined photoproduction and electroproduction data with the $\sigma_{LT'}$ data included were then generated. The first of these includes contributions from all of the resonances included in the previous study; the second excludes contributions from the $N(2080)$ and $N(2200)$ resonances. The results of both fits for both photoproduction and electroproduction observables are compared with the results of the previous fit and the data.

DOI: 10.1103/PhysRevC.86.064612 PACS number(s): 25.10.+s, 25.20.Lj, 25.30.Rw, 13.60.−r

I. INTRODUCTION

The production of strange baryons from the proton via the electromagnetic interaction has been a subject of intensive investigation for the last 25 years. Both the theoretical work [1–16] and the recent experimental work [17–24] have concentrated on the photoproduction reaction, but in the past few years there has been a renewal of interest in the electroproduction reaction generated by recent data from the Hall C collaboration [25] and from the CEBAF large acceptance spectrometer (CLAS) detector at the Thomas Jefferson National Accelerator Facility [26–29]. Electroproduction, while more difficult to study, is a potentially richer source of information than photoproduction in that it involves virtual photons rather than real photons and thus brings longitudinal degrees of freedom into play that are absent in the photoproduction process. Electroproduction also provides the possibility of studying hadronic electromagnetic form factors.

The earliest theoretical studies of electroproduction date from the mid 1970s and were based on a simple Regge model [30]. More recent studies generally employ an effective Lagrangian model [1–3,5,8,31,32], but there are also studies based on updated Regge models [33] and studies based on chiral frameworks [16,34].

Recently, a new fit to the data for both the electroproduction reaction $ep \to e'K^+\Lambda$ and the related photoproduction reaction $\gamma p \to K^+\Lambda$ was obtained using an effective Lagrangian model. This model [35] incorporates all of the well-established baryon resonances with spins up to $\frac{5}{2}$, four less-well-established nucleon resonances of higher mass, and the two kaon resonances $K^\star(892)$ and $K1(1270)$. In the electroproduction reaction, form factors were included at each hadron electromagnetic vertex. The model was fitted to photoproduction data from the CLAS [21–24], SAPHIR [17], LEPS [18], and GRAAL [19,20] collaborations and to electroproduction data from CLAS for the virtual photoproduction structure functions σ_U, σ_T, σ_L, σ_{TT}, and σ_{LT}.

In the present work, we extend the fit of Ref. [35] to include CLAS data for the structure function $\sigma_{LT'}$. This structure function is related to the beam polarization asymmetry and thus may provide information concerning the underlying dynamics of the reaction that is not attainable from the unpolarized structure functions alone. Fits that include polarization data also provide better starting points for investigations of reactions involving more complex targets such as the deuteron and ^{3}He.

The remainder of this work is organized as follows: in the next section, we define the matrix element for virtual photoproduction and discuss the structure functions that are usually employed to represent the virtual photoproduction cross section. Section III provides a summary of the virtual photoproduction reaction model. For a more detailed discussion of this model, the reader should consult Ref. [35]. Section IV presents details of the fitting procedure, including a summary of the data fit for both the photoproduction and electroproduction reactions and a list of the parameters that are fitted. Three sets of results are presented and discussed in Sec. V. The first was generated using the fit obtained in Ref. [35], which did not include $\sigma_{LT'}$ data in the fit, so that the $\sigma_{LT'}$ results obtained from that fit represent a prediction. The second set of results was generated from a fit that incorporated all of the resonances considered in Ref. [35] and which included the CLAS $\sigma_{LT'}$ data in the fit. Two of the resonances included in that fit, the negative-parity $N(2080)$ and $N(2200)$ resonances, have disappeared from the most recent particle data tables [36]. In order to ascertain the significance of these two resonances in the earlier fits, we have also obtained results from a fit in which contributions from these two resonances have been excluded.

II. VIRTUAL PHOTOPRODUCTION

Within the impulse approximation, the matrix element for the reaction $ep \to e'K^+\Lambda$ can be expressed in the form

$$\langle F \mid \hat{T} \mid I \rangle = \frac{l_\mu h^\mu}{q^2}, \tag{1}$$

where q is the virtual-photon four-momentum, l_μ is the lepton current given by

$$l_\mu = e\bar{u}_{M'}(p')\gamma_\mu u_M(p), \tag{2}$$

with p (p') and M (M') denoting the incident (final) electron four-momentum and spin projection, and h^μ is the hadron current given by

$$h^\mu = e\bar{u}_{M_\Lambda}(p_\Lambda)\hat{t}^\mu u_{M_p}(p_p). \tag{3}$$

For experiments where the helicity of the incident electron is measured, we need the square of this matrix element summed over the spin projections of the outgoing Λ and electron and averaged over the spin projection of the incident proton. After imposing current conservation,

$$q_\mu h^\mu = 0, \tag{4}$$

and treating the electron kinematics in the extreme relativistic approximation, this quantity can be reexpressed in terms of squares of the virtual photoproduction matrix element. In particular,

$$\frac{1}{2}\sum_{M_\Lambda M_p M'} |\langle F|\hat{T}|I\rangle|^2 = \frac{e^2}{4m_e^2 q^2}\frac{1}{\epsilon - 1}\sum_{M_\Lambda M_p} |\langle f|\hat{t}_\gamma|i\rangle|^2, \tag{5}$$

where the transverse photon polarization ϵ is given by

$$\epsilon = \left(1 - 2\frac{\mathbf{q}^2}{q^2}\tan^2\frac{\Psi}{2}\right)^{-1}, \tag{6}$$

with $\mathbf{q}$ denoting the spatial part of the virtual-photon momentum and Ψ denoting the electron scattering angle in the laboratory frame. The squares of the virtual photoproduction matrix element are in turn related to components of the hadron current, defined by Eq. (3), by the relation

$$\begin{aligned}
&\frac{1}{2}\sum_{M_\Lambda M_p} |\langle f|\hat{t}_\gamma|i\rangle|^2 \\
&= \frac{1}{4}\sum_{M_\Lambda M_p}\Big[(|h_x|^2 + |h_y|^2) + \epsilon(|h_x|^2 - |h_y|^2)\cos 2\phi \\
&\quad - 2\epsilon\frac{q^2}{q_0^2}|h_z|^2 - \frac{1}{q_0}\sqrt{-2q^2\epsilon(1+\epsilon)}(h_x h_z^\star + h_x^\star h_z)\cos\phi \\
&\quad + \frac{i\mathcal{H}}{q_0}\sqrt{-2q^2\epsilon(1-\epsilon)}(h_x h_z^\star - h_x^\star h_z)\sin\phi\Big],
\end{aligned} \tag{7}$$

where ϕ is the angle between the lepton and hadron planes, and the helicity of the incident electron $\mathcal{H}$ is defined to be $+1$ or -1 according to whether the incident electron spin projection is in the same direction or opposite to its three-momentum. Note here that the hadron current components are defined with respect to a coordinate system which has its z axis in the direction of the virtual-photon three-momentum and its x axis chosen so that the hadron three-momenta all lie in the xz plane with the x component of the kaon three-momentum positive.

In terms of the virtual photoproduction matrix elements, the virtual photoproduction cross section in the $K\Lambda$ c.m. system is given by

$$\frac{d\sigma_\gamma}{d\Omega_K} = \frac{1}{(8\pi)^2}\frac{m_p m_\Lambda p_K}{|\,\mathbf{q}\,|\,s}\frac{1}{2}\sum_{M_\Lambda M_p} |\langle f|\hat{t}_\gamma|i\rangle|^2, \tag{8}$$

where s is the square of the $K\Lambda$ c.m. energy. This expression can be decomposed into a set of structure functions according to the relation

$$\begin{aligned}
\frac{d\sigma_\gamma}{d\Omega_K} &= \sigma_T + \epsilon\sigma_L + \epsilon\sigma_{TT}\cos 2\phi + \sqrt{\epsilon(1+\epsilon)}\sigma_{LT}\cos\phi \\
&\quad + \mathcal{H}\sqrt{\epsilon(1-\epsilon)}\sigma_{LT'}\sin\phi,
\end{aligned} \tag{9}$$

where

$$\begin{aligned}
\sigma_T &= \frac{1}{4}k\sum_{M_\Lambda M_p}(|h_x|^2 + |h_y|^2), \\
\sigma_L &= \frac{1}{2}k\sum_{M_\Lambda M_p}\frac{-q^2}{q_0^2}|h_z|^2, \\
\sigma_{TT} &= \frac{1}{4}k\sum_{M_\Lambda M_p}(|h_x|^2 - |h_y|^2), \\
\sigma_{LT} &= -\frac{1}{2}k\sum_{M_\Lambda M_p}\frac{1}{q_0}\sqrt{-2q^2}Re(h_x h_z^\star), \\
\sigma_{LT'} &= -\frac{1}{2}k\sum_{M_\Lambda M_p}\frac{1}{q_0}\sqrt{-2q^2}Im(h_x h_z^\star),
\end{aligned} \tag{10}$$

with

$$k = \frac{m_p m_\Lambda p_K}{16\pi^2|\mathbf{q}|s}. \tag{11}$$

Because of the difficulty in separating the structure functions σ_T and σ_L experimentally, most of the available data related to these two structure functions is actually for the combination

$$\sigma_U = \sigma_T + \epsilon\sigma_L. \tag{12}$$

III. REACTION MODEL

The reaction model for the hadronic current includes three types of contributions, which are depicted in Fig. 1. These are usually labelled s-channel, u-channel, or t-channel contributions, according to whether the squared four-momentum in the intermediate state propagator corresponds to the s, t, or u Mandelstaam variable. The s-channel contributions include the Born term with an intermediate proton and contributions in which an intermediate nucleon resonance is excited. The u-channel contributions include the Born term with an intermediate Λ and terms with either a Σ baryon or an intermediate hyperon resonance. Finally, in the t channel, the Born contribution is supplemented with contributions involving both $K^\star(892)$ and $K1(1270)$ exchange.

The general structure of the hadron amplitude $\hat{t}^\mu$ depends upon the channel considered. For the s channel, we have

$$\hat{t}_s^\mu = \sum_{N^\star}[\mathcal{V}_K^\dagger(p_K)D(p_s)\mathcal{V}_\gamma(q)]^\mu, \tag{13}$$

where q is the virtual-photon four-momentum, $p_s = p_\Lambda + p_K$, and the $\mathcal{V}$ designate the interaction vertices and the D being the intermediate hadron propagators. The corresponding u- and t-channel expressions are

$$\hat{t}_u^\mu = \sum_{Y^\star}[\mathcal{V}_\gamma^\dagger(q)D(p_u)\mathcal{V}_K(p_K)]^\mu \tag{14}$$

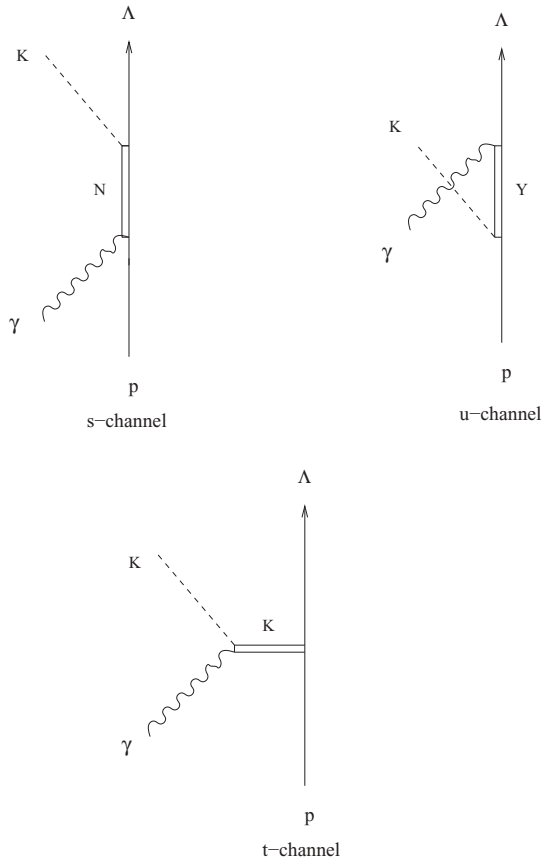

FIG. 1. Contributions to amplitude for reaction $\gamma p \to K^+\Lambda$.

and

$$\hat{t}_t^{\mu} = \sum_{K^\star} [\mathcal{V}^{\dagger}_{\gamma K}(q, p_t) D_t(p_t) \mathcal{V}_{p\Lambda}(p_t)]^{\mu}, \tag{15}$$

with $p_u = p_\Lambda - q$ and $p_t = q - p_K$.

The interaction vertices, as well as the propagators, depend upon the spin and parity of the intermediate hadron considered. In this work, we employ the same vertices and propagators as were discussed in Ref. [35], but in that work, the vertices were given for the photoproduction reaction. Here we list the vertices appropriate for the electroproduction reaction.

In the s and u channels, the positive-parity electromagnetic interaction vertices are given by (with form factors suppressed)

$$\begin{aligned}
\mathcal{V}^{\mu}_{\gamma \frac{1}{2}^+}(q) &= \frac{e\kappa}{2m_B} i\sigma^{\mu\nu} q_\nu, \\
\mathcal{V}^{\mu\nu}_{\gamma \frac{3}{2}^+}(q) &= \left[\frac{g_1}{2m_B} (\gamma \cdot q g^{\mu\nu} - \gamma^\mu q^\nu) \right. \\
&\quad \left. + \frac{g_2}{4m_B^2} \left(p_B^\mu q^\nu - q \cdot p_B g^{\mu\nu} \right) \right] \gamma_5, \\
\mathcal{V}^{\mu\nu\alpha}_{\gamma \frac{5}{2}^+}(q) &= \left[\frac{g_1}{2m_B} (\gamma \cdot q g^{\mu\nu} - \gamma^\mu q^\nu) \right. \\
&\quad \left. + \frac{g_2}{4m_B^2} \left(p_B^\mu q^\nu - q \cdot p_B g^{\mu\nu} \right) \right] q^\alpha,
\end{aligned} \tag{16}$$

where m_B and p_B are the mass and four-momentum of the incident proton in the s channel and the mass and four-momentum of the outgoing Λ in the u channel. In the expression for the spin-$\frac{1}{2}$ vertex, κ is defined by its relation to the transition magnetic moment,

$$\mu_T = \frac{e\kappa}{m_B + m_I}, \tag{17}$$

where m_I is the mass of the intermediate baryon. The Born terms in both channels have an additional charge contribution given by

$$\mathcal{V}^{\mu}_{\text{charge}} = e\gamma^\mu. \tag{18}$$

Note that in photoproduction, which involves a physical photon, current conservation requires that the charge contribution in the u-channel vanish because the outgoing Λ is neutral. Thus in electroproduction, the form factor that multiplies the u-channel charge contribution must vanish when the incident photon is on shell.

In the t channel, the positive-parity electromagnetic interaction vertices are given by (again with form factors suppressed)

$$\begin{aligned}
\mathcal{V}^{\mu}_{\gamma K} &= e\left(2p_K^\mu - q^\mu\right), \\
\mathcal{V}^{\mu\nu}_{\gamma K(892)} &= \frac{g_{\gamma K K^\star}}{m_{sc}} \epsilon^{\mu\alpha\beta\nu} q_\alpha p_{t\beta}, \\
\mathcal{V}^{\mu\nu}_{\gamma K(1270)} &= \frac{g_{\gamma K K1}}{m_{sc}} \left(p_t^\mu q^\nu - q \cdot p_t g^{\mu\nu} \right),
\end{aligned} \tag{19}$$

where p_t is the four-momentum of the intermediate kaon or kaon resonance, and m_{sc} is a scaling mass, set equal to 1 GeV, introduced to make the electromagnetic coupling strengths dimensionless.

The corresponding expressions for the strong interaction vertices are

$$\begin{aligned}
\mathcal{V}_{K \frac{1}{2}^+}(p_K) &= g\gamma_5, \\
\mathcal{V}^{\mu}_{K \frac{3}{2}^+}(p_K) &= -\frac{g}{m_\pi} p_K^\mu, \\
\mathcal{V}^{\mu\nu}_{K \frac{5}{2}^+}(p_K) &= \frac{g}{m_\pi^2} p_K^\mu p_K^\nu \gamma_5,
\end{aligned} \tag{20}$$

in the s and u channels for positive-parity intermediate baryons and

$$\begin{aligned}
\mathcal{V}_{p\Lambda K} &= g_{\Lambda K p}\gamma_5, \\
\mathcal{V}^{\mu}_{p\Lambda K(892)} &= \left(g^V_{\Lambda K^\star p} + \frac{g^T_{\Lambda K^\star p}}{m_p + m_\Lambda} \gamma \cdot p_t \right) \gamma^\mu, \\
\mathcal{V}^{\mu}_{p\Lambda K(1270)} &= \left(g^V_{\Lambda K1 p} + \frac{g^T_{\Lambda K1 p}}{m_p + m_\Lambda} \gamma \cdot p_t \right) \gamma^\mu \gamma_5,
\end{aligned} \tag{21}$$

in the t channel. In the s and u channels the interaction vertices for negative-parity intermediate baryons are just the positive-parity expressions with the γ_5 factor transposed from the strong interaction vertex to the electromagnetic vertex.

For the spin-$\frac{1}{2}$ propagator in the s and u channels, we employ, in agreement with other authors, a relativistic Breit-Wigner form,

$$D^{\frac{1}{2}}(p) = \frac{\gamma \cdot p + m_I}{p^2 - m_I^2 + i m_I \Gamma_I}, \tag{22}$$

where, as above, m_I is the mass of the intermediate baryon, and the corresponding width Γ_I is nonzero only in the s channel. The propagators for the higher spin states are then obtained by multiplying the spin-$\frac{1}{2}$ propagator by the appropriate spin projection operator. Thus,

$$D^{\frac{3}{2}}_{\mu\nu}(p) = D^{\frac{1}{2}} P^{\frac{3}{2}}_{\mu\nu}, \quad D^{\frac{5}{2}}_{\mu\nu\alpha\beta}(p) = D^{\frac{1}{2}} P^{\frac{5}{2}}_{\mu\nu\alpha\beta}, \tag{23}$$

with

$$\begin{aligned} P^{\frac{3}{2}}_{\mu\nu} &= g_{\mu\nu} - \frac{1}{3}\gamma_\mu\gamma_\nu + \frac{1}{3}\frac{p_\mu\gamma_\nu - p_\nu\gamma_\mu}{m_I} - \frac{2}{3}\frac{p_\mu p_\nu}{m_I^2}, \\ P^{\frac{5}{2}}_{\mu\nu\alpha\beta} &= R_{\mu\nu\alpha\beta} - \frac{1}{5}P_{\mu\nu}P_{\alpha\beta} - \frac{1}{5}(P_{\mu\rho}\gamma^\rho\gamma^\sigma R_{\sigma\nu\alpha\beta} \\ &\quad + P_{\nu\rho}\gamma^\rho\gamma^\sigma R_{\sigma\mu\alpha\beta}), \end{aligned} \tag{24}$$

where

$$R_{\mu\nu\alpha\beta} = \tfrac{1}{2}(P_{\mu\alpha}P_{\nu\beta} + P_{\mu\beta}P_{\nu\alpha}), \tag{25}$$

and

$$P_{\mu\nu} = g_{\mu\nu} - p_\mu p_\nu / m_I^2. \tag{26}$$

In the t channel, the kaon propagator is simply

$$D_t = \left[p_t^2 - m_I^2\right]^{-1}. \tag{27}$$

Multiplication by the spin-1 projection operator,

$$P^1_{\mu\nu} = -g_{\mu\nu} + \frac{p_{t\mu}p_{t\nu}}{m^2_{K^\star}}, \tag{28}$$

yields the $K^\star(892)$ and $K1(1270)$ propagators, where now the label $K^\star$ refers to either kaon resonance.

The nucleon resonances excited in the s channel generally lie in kinematic regions where various decay channels are open. It is thus necessary to include widths in the s-channel resonance propagators, and these widths are often required rather far off the resonance mass shell. In this work, we employ the same dynamical model for the widths that was used in Ref. [35]. Within that model, the width of each intermediate nucleon resonance is decomposed into partial widths. The energy and momentum dependence of each partial width is generated using an effective Lagrangian model with the required coupling strengths adjusted to reproduce the empirical on-shell branching ratios. Decay channels involving more than two decay products are approximated as two-body decays with one unstable decay product the mass distribution of which is represented by a Breit-Wigner distribution function. A more detailed description of the model, including expressions for the phase-space factors and the distribution function employed together with values for all the branching ratios employed, may be found in Ref. [10].

The width model summarized above is suitable for well-established resonances where there is enough branching ratio data to provide reasonably good estimates of the on-shell partial widths. For the less-well-established nucleon resonances of higher mass, these data are absent. Hence, for these resonances, the energy and momentum dependence of the widths is ignored, and the values given in Ref. [10] adopted.

Because the exchanged photon is off shell, it is necessary in effective Lagrangian treatments of electroproduction to include form factors at all the electromagnetic vertices in the reaction amplitude. Here, we employ the same form factors as were used in Ref. [35]. In that work, in contrast with earlier work, a separate form factor was employed for each intermediate baryon in the s and u channels.

In the Born terms, both charge and magnetic form factors are required. For the proton, the form factors obtained by Gari and Krupelmann [37] based on a modified vector dominance model are employed. Details concerning this model, including parameter values, can be found in Ref. [32].

For the u-channel Born contribution, the charge and magnetic form factors are given by the linear combinations

$$\begin{aligned} F_C(q^2) &= F_{\Lambda 1}(q^2) - \tau_\Lambda F_{\Lambda 2}(q^2), \\ F_M(q^2) &= \frac{1}{\kappa_\Lambda}[F_{\Lambda 1}(q^2) + F_{\Lambda 2}(q^2)], \end{aligned} \tag{29}$$

where

$$\tau_\Lambda = \frac{q^2}{4m_\Lambda^2}. \tag{30}$$

The form factors $F_{\Lambda 1}$ and $F_{\Lambda 2}$ are, in turn, expressed as linear combinations of two other form factors,

$$\begin{aligned} F_{\Lambda 1}(q^2) &= \frac{1}{2}[F_1(q^2) - F_2(q^2)], \\ F_{\Lambda 2}(q^2) &= \frac{\kappa_\Lambda}{2}[F_1(q^2) + F_2(q^2)], \end{aligned} \tag{31}$$

which are assumed to have the same functional form,

$$F_i\left(q^2\right) = \frac{1}{1+\alpha_i}\frac{\Lambda_i^2}{\Lambda_i^2 - q^2}\left(1 + \alpha_i\frac{\Lambda_i^2}{\Lambda_i^2 - q^2}\right), \tag{32}$$

but with different values for the parameters α_i and Λ_i.

The s- and u-channel contributions with intermediate resonance states each require just a single electromagnetic form factor. For these form factors, the expression given by Eq. (32) is used with separate values for α and Λ employed for each resonance.

In the t-channel Born term, we make use of a parametrization based on a relativistic quark model [38]. It is given by

$$F_K\left(q^2\right) = \alpha_K\frac{\Lambda_1^2}{\Lambda_1^2 - q^2} + (1-\alpha_K)\left(\frac{\Lambda_2^2}{\Lambda_2^2 - q^2}\right)^2, \tag{33}$$

with $\alpha_K = 0.398$, $\Lambda_1 = 0.642$ GeV, and $\Lambda_2 = 1.386$ GeV. For the resonant contributions in the t channel, the form

$$F_{K^\star}(q^2) = \frac{\Lambda^2_{K^\star}}{\Lambda^2_{K^\star} - q^2}, \tag{34}$$

is used.

In the absence of form factors, the Born charge contributions collectively satisfy the current conservation condition. This collective satisfaction of current conservation is disrupted when form factors are included. To restore it, it is necessary to add counter terms to the charge contributions in such a way that the on-shell limits of these contributions are not altered. Here we employ the same prescription as was used in Ref. [35]; namely, the charge contributions to $\hat{t}^\mu$ are

TABLE I. Baryon resonances considered in the model.

Resonance	I	J^P
$N(1440)$	$\frac{1}{2}$	$\frac{1}{2}^+$
$N(1520)$	$\frac{1}{2}$	$\frac{3}{2}^-$
$N(1535)$	$\frac{1}{2}$	$\frac{1}{2}^-$
$N(1650)$	$\frac{1}{2}$	$\frac{1}{2}^-$
$N(1675)$	$\frac{1}{2}$	$\frac{5}{2}^-$
$N(1680)$	$\frac{1}{2}$	$\frac{5}{2}^+$
$N(1700)$	$\frac{1}{2}$	$\frac{3}{2}^-$
$N(1710)$	$\frac{1}{2}$	$\frac{1}{2}^+$
$N(1720)$	$\frac{1}{2}$	$\frac{3}{2}^+$
$N(1900)$	$\frac{1}{2}$	$\frac{3}{2}^+$
$N(2000)$	$\frac{1}{2}$	$\frac{5}{2}^+$
$N(2080)$	$\frac{1}{2}$	$\frac{3}{2}^-$
$N(2200)$	$\frac{1}{2}$	$\frac{5}{2}^-$
$\Lambda(1405)$	0	$\frac{1}{2}^-$
$\Lambda(1670)$	0	$\frac{1}{2}^-$
$\Lambda(1820)$	0	$\frac{5}{2}^+$
$\Lambda(1830)$	0	$\frac{5}{2}^-$
$\Lambda(1890)$	0	$\frac{3}{2}^+$
$\Lambda(2110)$	0	$\frac{5}{2}^+$
$\Sigma(1385)$	1	$\frac{3}{2}^+$
$\Sigma(1775)$	1	$\frac{5}{2}^-$
$\Sigma(1915)$	1	$\frac{5}{2}^+$
$\Sigma(1940)$	1	$\frac{3}{2}^-$

replaced by the expressions

$$\hat{t}^{\mu}_{s,\mathrm{ch}} = eF_C(q^2)\gamma^{\mu} + e[1-F_C(q^2)]\frac{q^{\mu}}{q^2}\gamma\cdot q,$$
$$\hat{t}^{\mu}_{u,\mathrm{ch}} = eF_C(q^2)\left[\gamma^{\mu} - \frac{q^{\mu}}{q^2}\gamma\cdot q\right],$$
$$\hat{t}^{\mu}_{t,\mathrm{ch}} = eF_K(q^2)\left(2p_K^{\mu} - q^{\mu}\right) + e[1-F_K(q^2)] \times \left(\frac{2p_K\cdot q}{q^2} - 1\right)q^{\mu}. \quad (35)$$

With the exception of the $K^\star(892)$ resonance contribution to the t channel, the spatial parts of the hadronic current amplitudes discussed above all have the general structure

$$\hat{\mathbf{t}} = \alpha_{\mathbf{1}} + \alpha_{\mathbf{2}}\gamma_5 + \alpha_{\mathbf{3}}\gamma^0 + \alpha_{\mathbf{4}}\gamma^0\gamma_5 + D_1\gamma + D_2\gamma\gamma_5 + D_3\gamma^0\gamma + D_4\gamma^0\gamma\gamma_5, \quad (36)$$

where the vector operators α and the scalar operators D are momentum-dependent operators that act within the baryon 2×2 Pauli spinor space. The corresponding form for the t-channel $K^\star(892)$ contribution is

$$\hat{\mathbf{t}} = \alpha_{\mathbf{1}} + \alpha_{\mathbf{2}}\gamma_5 + \alpha_{\mathbf{3}}\gamma^0 + \alpha_{\mathbf{4}}\gamma^0\gamma_5 + \beta_{\mathbf{1}}\times\gamma + \beta_{\mathbf{2}}\times\gamma\gamma_5 + \beta_{\mathbf{3}}\times\gamma^0\gamma + \beta_{\mathbf{4}}\times\gamma^0\gamma\gamma_5. \quad (37)$$

Detailed expressions for these operators can be found in the appendix of Ref. [35]. The matrix elements of the $\hat{\mathbf{t}}$ between Dirac spinors were evaluated numerically, as was done in Ref. [35].

TABLE II. Fit results for the coupling-strength products. For each hadron, the first set of numbers is from the first of the fits described here, which incorporates data for $\sigma_{LT'}$. The second set is from the fit that excludes the $N(2080)$ and $N(2200)$ resonances but incorporates $\sigma_{LT'}$ data, while the third set is from Ref. [35], which does not incorporate $\sigma_{LT'}$ data.

		Spin-$\frac{1}{2}$ resonances		
$N(1440)$	$F_{N^\star}$	2.5489	2.6909	3.2545
$N(1535)$	$F_{N^\star}$	0.4432	0.4267	0.4375
$N(1650)$	$F_{N^\star}$	−0.0699	−0.0684	−0.0484
$N(1710)$	$F_{N^\star}$	0.0633	0.0690	0.0941
$\Lambda(1405)$	$F_{\Lambda^\star}$	−3.2449	−3.2050	−3.2802
$\Lambda(1670)$	$F_{\Lambda^\star}$	4.5245	4.2239	4.4016
		Spin-$\frac{3}{2}$ resonances		
$N(1520)$	$G^1_{N^\star}$	−0.8056	−0.8292	−0.7442
	$G^2_{N^\star}$	−0.3810	−0.3994	−0.5355
$N(1700)$	$G^1_{N^\star}$	−0.0498	−0.0615	−0.0970
	$G^2_{N^\star}$	−0.2314	−0.2801	−0.0675
$N(1720)$	$G^1_{N^\star}$	−0.0074	−0.0012	−0.0020
	$G^2_{N^\star}$	−0.3853	−0.3815	−0.3068
$N(1900)$	$G^1_{N^\star}$	0.0362	0.0359	0.0210
	$G^2_{N^\star}$	0.0157	0.0157	−0.0146
$N(2080)$	$G^1_{N^\star}$	−0.0132		−0.0066
	$G^2_{N^\star}$	−0.0063		0.0012
$\Lambda(1890)$	$G^1_{\Lambda^\star}$	−1.2877	−1.3007	−1.6976
	$G^2_{\Lambda^\star}$	−8.6660	−8.5795	−7.9940
$\Sigma(1385)$	$G^1_{\Sigma^\star}$	−0.1478	−0.1074	0.1278
	$G^2_{\Sigma^\star}$	6.3399	6.5442	5.3970
$\Sigma(1940)$	$G^1_{\Sigma^\star}$	1.6764	1.8796	1.3050
	$G^2_{\Sigma^\star}$	0.0650	0.3311	0.2441
		Spin-$\frac{5}{2}$ resonances		
$N(1675)$	$G^1_{N^\star}$	−0.0041	−0.0046	−0.0031
	$G^2_{N^\star}$	−0.0087	−0.0126	−0.0095
$N(1680)$	$G^1_{N^\star}$	0.0273	0.0274	0.0251
	$G^2_{N^\star}$	0.0039	0.0035	0.0012
$N(2000)$	$G^1_{N^\star}$	−0.0137	−0.0143	−0.0172
	$G^2_{N^\star}$	−0.0085	−0.0095	−0.0110
$N(2200)$	$G^1_{N^\star}$	−0.0003		−0.0001
	$G^2_{N^\star}$	−0.0023		−0.0004
$\Lambda(1820)$	$G^1_{\Lambda^\star}$	−0.1733	−0.1725	−0.1643
	$G^2_{\Lambda^\star}$	−1.3258	−1.3133	−1.8779
$\Lambda(1830)$	$G^1_{\Lambda^\star}$	−0.1190	−0.1166	−0.0875
	$G^2_{\Lambda^\star}$	−0.4265	−0.3926	−0.1653
$\Lambda(2110)$	$G^1_{\Lambda^\star}$	−0.1743	−0.1560	−0.1539
	$G^2_{\Lambda^\star}$	−1.2997	−1.2795	−1.5859
$\Sigma(1775)$	$G^1_{\Sigma^\star}$	0.1015	0.1001	0.0730
	$G^2_{\Sigma^\star}$	0.4371	0.4068	0.1749
$\Sigma(1915)$	$G^1_{\Sigma^\star}$	0.3496	0.3340	0.3204
	$G^2_{\Sigma^\star}$	2.5639	2.5342	3.4085
		t-channel resonances		
$K(892)$	$G^V_{K^\star}$	3.2244	3.1835	3.2840
	$G^T_{K^\star}$	1.4557	1.6769	0.9215
$K(1270)$	$G^V_{K^\star}$	1.4544	1.5024	1.3698
	$G^T_{K^\star}$	−1.4401	−0.9890	−3.4497

TABLE III. Fit results for the electromagnetic form factor parameters. For each hadron, the first pair of numbers is from the first of the fits described here, which incorporates data for $\sigma_{LT'}$, the second pair is from the fit that excludes the $N(2080)$ and $N(2200)$ resonances but incorporates $\sigma_{LT'}$ data, while the third pair is from Ref. [35], which does not incorporate $\sigma_{LT'}$ data.

	Λ	α	Λ	α	Λ	α
			Spin-$\frac{1}{2}$ resonances			
$N(1440)$	0.3578	4.8705	0.3578	4.8705	1.4572	2.8997
$N(1535)$	1.7219	4.5155	1.7029	4.5155	1.6180	4.5155
$N(1650)$	4.4379	−4.8632	4.4379	−4.8632	4.6512	−4.8632
$N(1710)$	4.0544	4.0269	4.0544	4.0269	2.6098	4.0269
$F_1(\Lambda)$	1.2900	4.9810	1.2848	4.9737	1.4653	0.7876
$F_2(\Lambda)$	4.9790	−1.3335	4.9790	−1.3445	4.7441	−1.4324
$\Lambda(1405)$	2.2452	−0.8471	2.2961	−0.8464	2.8688	−0.4031
$\Lambda(1670)$	0.3477	−0.1943	0.3368	−0.1538	0.2707	−0.5281
Σ	1.9481	−0.9526	1.9300	−0.9518	1.8314	−0.8612
			Spin-$\frac{3}{2}$ resonances			
$N(1520)$	1.7576	3.4965	1.7450	3.4965	1.7213	3.4965
$N(1700)$	2.3527	−1.5142	2.4139	−1.4940	3.7186	−3.8566
$N(1720)$	1.3866	3.7758	1.4104	3.7758	1.5354	3.7758
$N(1900)$	4.8314	−1.2346	4.8314	−1.2346	4.6720	−1.3748
$N(2080)$	4.1062	2.6698			4.2171	2.6698
$\Lambda(1890)$	0.3723	0.0471	0.3789	0.0208	0.4491	−0.0360
$\Sigma(1385)$	0.5913	4.3992	0.6027	4.3992	0.7034	4.0338
$\Sigma(1940)$	0.3433	0.0958	0.3449	0.1316	0.2584	2.3431
			Spin-$\frac{5}{2}$ resonances			
$N(1675)$	1.2338	4.8271	1.2417	4.8271	1.1856	4.8271
$N(1680)$	1.2083	3.2090	1.2080	3.2090	1.1045	1.0577
$N(2000)$	1.3310	2.7443	1.2272	2.7443	1.4616	3.6176
$N(2200)$	4.8669	−2.8773			3.3698	−2.8773
$\Lambda(1820)$	1.0939	2.3327	1.0914	2.3351	1.1050	2.4088
$\Lambda(1830)$	0.2271	3.0470	0.2271	3.0470	0.2133	1.6144
$\Lambda(2110)$	0.4807	−0.4587	0.4831	−0.4584	0.5460	−0.4098
$\Sigma(1775)$	0.3071	4.7806	0.3029	4.7806	0.2576	3.0308
$\Sigma(1915)$	1.0007	1.5498	1.0025	1.5652	1.0454	1.6727

	$\Lambda_{K^\star}$	$\Lambda_{K^\star}$	$\Lambda_{K^\star}$
		t-channel resonances	
$K(892)$	0.284	0.280	0.211
$K(1270)$	0.894	0.921	0.672

IV. FITTING PROCEDURE

The nucleon and hyperon resonances considered in the fits presented here are listed in Table I. In the earlier photoproduction fit of Ref. [10], a larger set of u-channel resonances was initially considered, but it was found that a better fit was achieved with the reduced set of u-channel resonances employed here.

The set of parameters varied in the fit includes the products of the coupling strengths at the two interaction vertices in each resonance contribution to the reaction amplitude. These products are defined by the relations

$$F_{N^\star} = e\kappa_{pN^\star} g_{\Lambda K N^\star}, \quad F_{\Lambda^\star} = e\kappa_{\Lambda\Lambda^\star} g_{\Lambda^\star K p}, \quad F_{\Sigma^\star} = e\kappa_{\Lambda\Sigma^\star} g_{\Sigma^\star K p}, \tag{38}$$

TABLE IV. χ^2 per data point for various sets of data. For each data set, the first value is from the first fit described here, which incorporates data for $\sigma_{LT'}$, the second value is from the fit that excludes the $N(2080)$ and $N(2200)$ resonances but incorporates $\sigma_{LT'}$ data, while the third value is from Ref. [35], which does not incorporate $\sigma_{LT'}$ data.

Data set	χ^2	χ^2	χ^2
Photoproduction data	2.852	2.149	2.263
Electroproduction data	4.878	4.356	4.625
$\sigma_{LT'}$ data	14.26	11.78	11.48

for the spin-$\frac{1}{2}$ resonances in the s and u channels, by

$$G^1_{N^\star} = g_1^{pN^\star} g_{\Lambda K N^\star}, \quad G^2_{N^\star} = g_2^{pN^\star} g_{\Lambda K N^\star},$$
$$G^1_{\Lambda^\star} = g_1^{\Lambda\Lambda^\star} g_{\Lambda^\star K p}, \quad G^2_{\Lambda^\star} = g_2^{\Lambda\Lambda^\star} g_{\Lambda^\star K p}, \tag{39}$$
$$G^1_{\Sigma^\star} = g_1^{\Lambda\Sigma^\star} g_{\Sigma^\star K p}, \quad G^2_{\Sigma^\star} = g_2^{\Lambda\Sigma^\star} g_{\Sigma^\star K p},$$

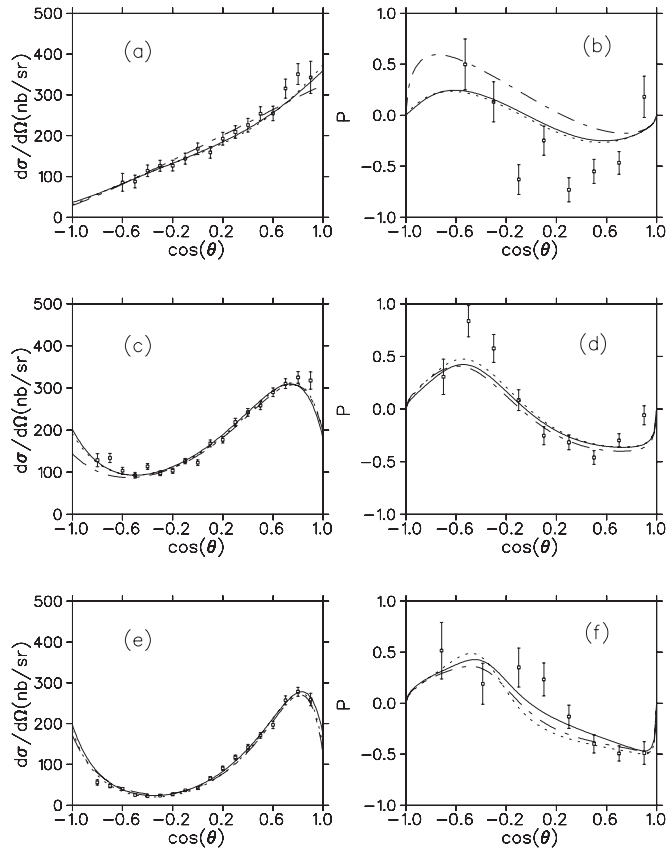

FIG. 2. Differential cross section vs $\cos(\theta)$ for (a) $W = 1.727$ GeV, (c) $W = 1.920$ GeV, and (e) $W = 2.120$ GeV, and the hyperon polarization asymmetry vs $\cos(\theta)$ for (b) $W = 1.730$ GeV, (d) $W = 1.934$ GeV, and (f) $W = 2.029$ GeV, where θ is the c.m. scattering angle and W is the c.m. energy. The solid curves were obtained from the first fit described in this work, the dotted curves were obtained from the fit that excludes the $N(2080)$ and $N(2200)$ resonances, and the dot-dashed curves are from the fit of Ref. [35]. Cross-section data are from Ref. [23], and polarization data are from Ref. [21].

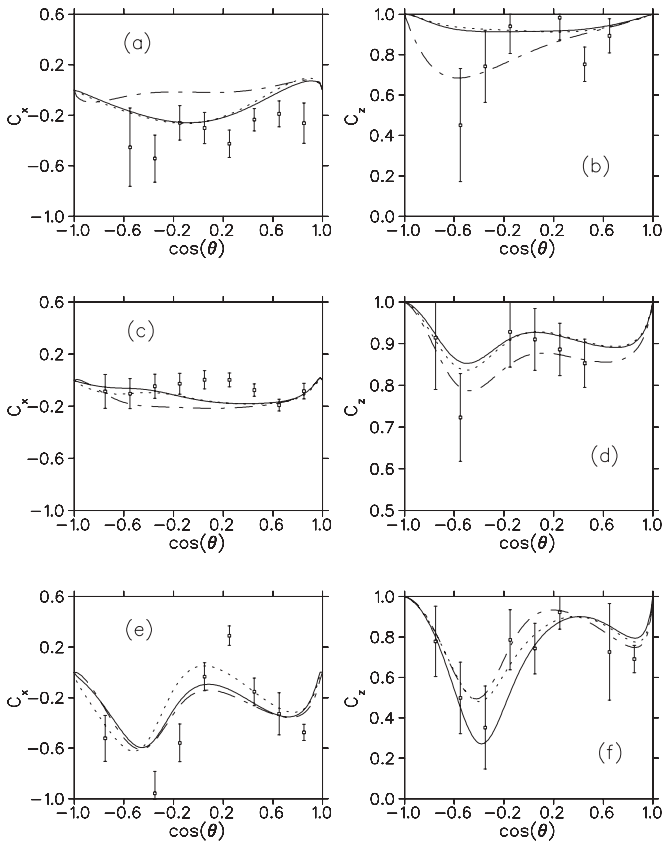

FIG. 3. C_x vs $\cos(\theta)$ for (a) $W = 1.734$ GeV, (c) $W = 1.939$ GeV, and (e) $W = 2.126$ GeV, and C_z vs $\cos(\theta)$ for (b) $W = 1.734$ GeV, (d) $W = 1.939$ GeV, and (f) $W = 2.126$ GeV, where θ is the c.m. scattering angle and W is the c.m. energy. Curve identification is as in Fig. 2. Data are from Ref. [24].

for the spin-$\frac{3}{2}$ and spin-$\frac{5}{2}$ resonances in the s and u channels, and by

$$G^V_{K^\star} = g_{\gamma K K^\star} g^V_{\Lambda K^\star p},$$
$$G^T_{K^\star} = g_{\gamma K K^\star} g^T_{\Lambda K^\star p}, \tag{40}$$

for the t-channel kaon resonances, where $e = 0.3029$ is the dimensionless electric charge.

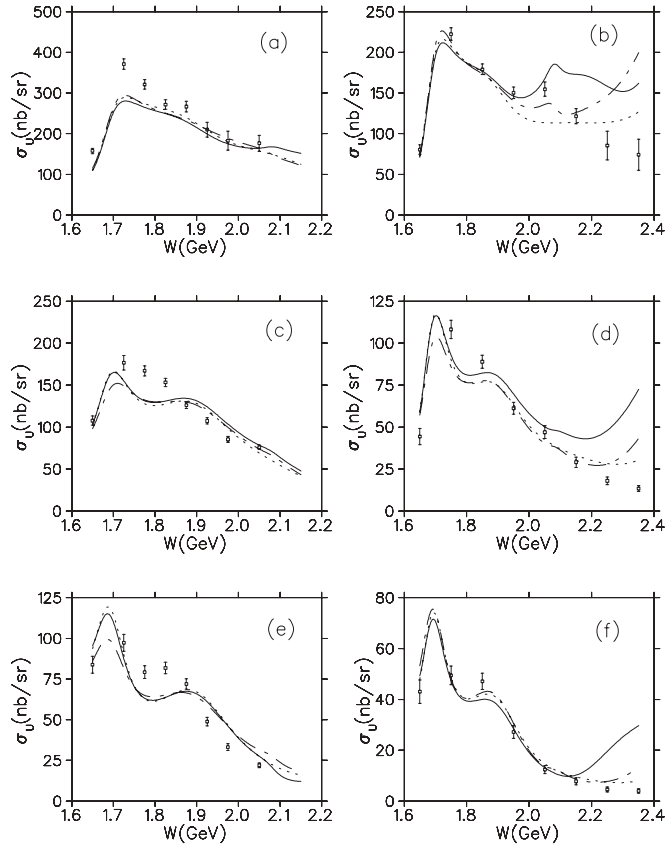

FIG. 5. σ_U vs W for (a) $\cos(\theta) = 0.90$ and $-q^2 = 0.65$ GeV^2, (b) $\cos(\theta) = 0.90$ and $-q^2 = 1.55$ GeV^2, (c) $\cos(\theta) = 0.35$ and $-q^2 = 0.65$ GeV^2, (d) $\cos(\theta) = 0.35$ and $-q^2 = 1.55$ GeV^2, (e) $\cos(\theta) = -0.25$ and $-q^2 = 0.65$ GeV^2, and (f) $\cos(\theta) = -0.25$ and $-q^2 = 1.55$ GeV^2, where θ and W are the scattering angle and energy in the $K\Lambda$ c.m. frame, respectively, and q^2 is the square of the virtual-photon four-momentum. The $-q^2 = 0.65$ GeV^2 results were obtained with $E = 2.567$ GeV and the $-q^2 = 1.55$ GeV^2 results with $E = 4.056$ GeV, where E is the energy of the incident electron in the laboratory frame. Curve identification is as in Fig. 2. Data are from Ref. [27].

For the Born term coupling products and for the u-channel term with an intermediate Σ, we employ the same fixed values

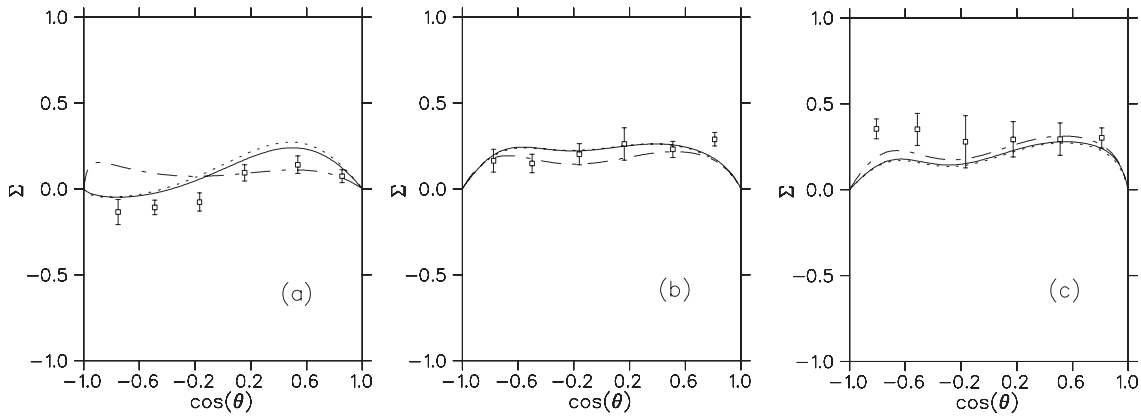

FIG. 4. Photon-beam asymmetry vs $\cos(\theta)$ for (a) $W = 1.702$ GeV, (b) $W = 1.808$ GeV, and (c) $W = 1.906$ GeV, where θ is the c.m. scattering angle and W is the c.m. energy. Curve identification is as in Fig. 2. Data are from Ref. [19].

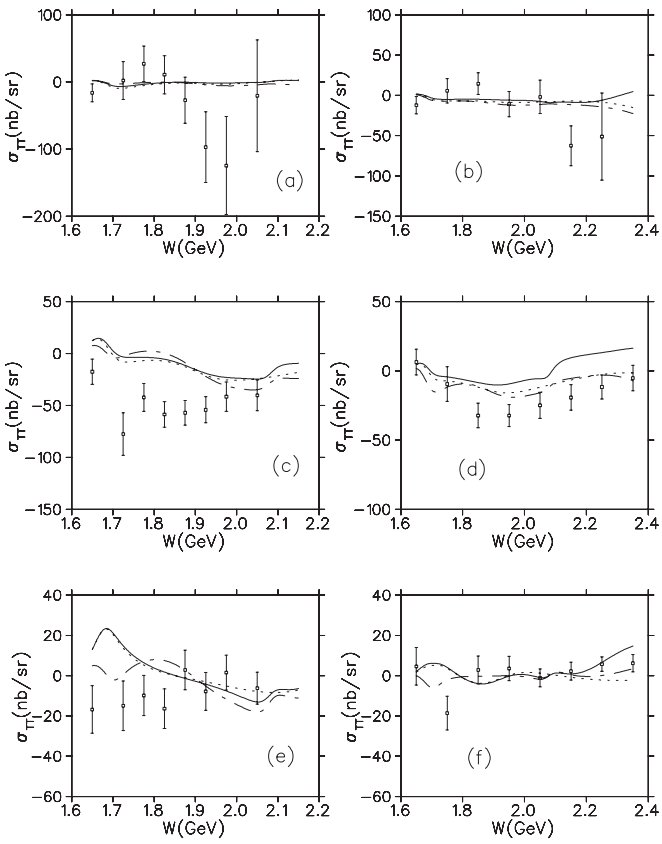

FIG. 6. σ_{TT} vs W for the same values of $\cos(\theta)$ and $-q^2$ as in Fig. 5, where θ and W are the scattering angle and energy in the $K\Lambda$ c.m. frame, and q^2 is the square of the virtual-photon four-momentum. Curve identification is as in Fig. 2. Data are from Ref. [27].

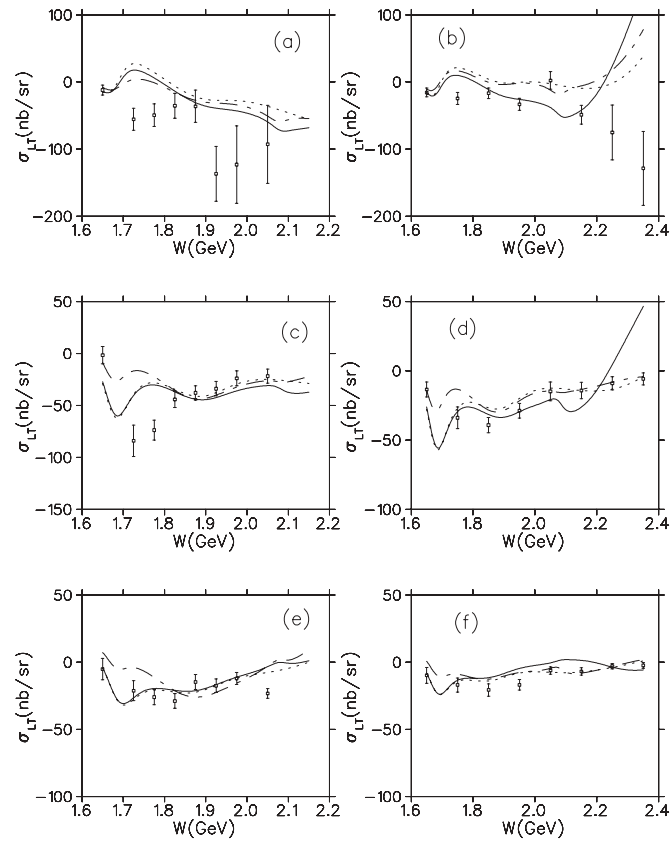

FIG. 7. σ_{LT} vs W for the same values of $\cos(\theta)$ and $-q^2$ as in Fig. 5, where θ and W are the scattering angle and energy in the $K\Lambda$ c.m. frame, and q^2 is the square of the virtual-photon four-momentum. Curve identification is as in Fig. 2. Data are from Ref. [27].

that were used in Ref. [35]; namely,

$$\begin{aligned} F_{Cp} &= eg_{\Lambda Kp} = -1.98, \\ F_p &= \kappa_p F_{Cp} = -3.54, \\ F_{C\Lambda} &= F_{Cp} = -1.98, \\ F_\Lambda &= \kappa_\Lambda F_{Cp} = 1.44, \\ F_\Sigma &= \frac{1}{\sqrt{3}} \frac{1-2\alpha}{1-\frac{2}{3}\alpha} \frac{\kappa_{\Lambda\Sigma}}{\kappa_\Lambda} F_\Lambda = 0.934, \\ F_K &= F_{Cp} = -1.98, \end{aligned} \tag{41}$$

where F_{Cp} and $F_{C\Lambda}$ are the Born charge coupling products, and F_p, F_Λ, and F_K are the Born magnetic coupling products. Note that the form factor that multiplies $F_{C\Lambda}$ is zero in the physical photon limit.

In addition to the resonance-coupling products, the fitted parameters also include the mass and coupling parameters associated with the electromagnetic form factors given by Eqs. (32) and (34).

As in Ref. [35], the large number of fitted parameters required a two-step procedure. Beginning with the fit of Ref. [35], we first refitted the resonance coupling products to the full set of photoproduction data considered in Ref. [35] along with CLAS data [27] for the virtual photoproduction structure functions defined by Eqs. (9) and (12), including the $\sigma_{LT'}$ data not included in the fit of Ref. [35]. The photoproduction data incorporated consists of CLAS data for the differential cross section [23]; CLAS [21], SAPHIR [17], and GRAAL [19] data for the hyperon polarization asymmetry P defined by

$$P = \frac{d\sigma_\Lambda^+ - d\sigma_\Lambda^-}{d\sigma_\Lambda^+ + d\sigma_\Lambda^-}, \tag{42}$$

where the superscripts $^+$ and $^-$ refer to spin projections above and below the scattering plane, respectively; GRAAL [19] and LEPS [18] data for the photon beam asymmetry Σ defined by

$$\Sigma = \frac{d\sigma_\Lambda^\perp - \sigma_\Lambda^\parallel}{d\sigma_\Lambda^\perp + \sigma_\Lambda^\parallel}, \tag{43}$$

where $\perp$ and $\parallel$ refer to polarization vectors perpendicular and parallel to the scattering plane, respectively; and CLAS [24] data for the double polarization observables C_x and C_z defined by

$$C_i = \frac{d\sigma_\Lambda^+ - d\sigma_\Lambda^-}{d\sigma_\Lambda^+ + d\sigma_\Lambda^-}, \tag{44}$$

where now the superscripts $^+$ and $^-$ refer to Λ spin projections along and opposite to the $i = z$ or $i = x$ axes, and the incident photon is circularly polarized with positive helicity. Using the new set of coupling strength products so obtained, we then refitted the electromagnetic form factor parameters to the virtual photoproduction data. The new form factor parameters

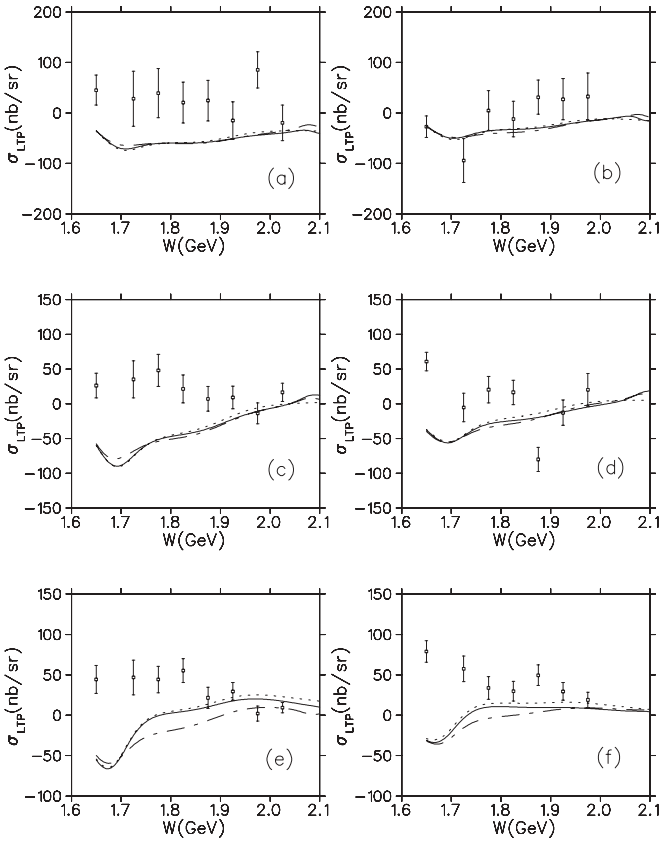

FIG. 8. $\sigma_{LT'}$ vs W for the same values of $\cos(\theta)$ as in Fig. 5 and for $-q^2 = 0.65$ GeV^2 in panels (a), (c), and (e), and $-q^2 = 1.00$ GeV^2 in panels (b), (d), and (f), where θ and W are the scattering angle and energy in the $K\Lambda$ c.m. frame, and q^2 is the square of the virtual-photon four-momentum. Curve identification is as in Fig. 2. Data are from Ref. [28].

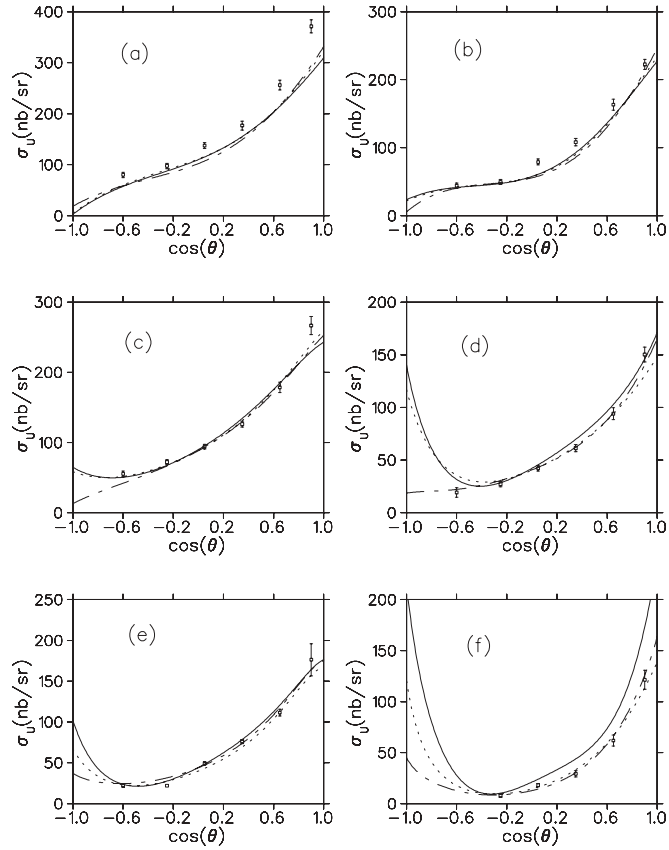

FIG. 9. σ_U vs $\cos(\theta)$ for (a) $W = 1.725$ GeV and $-q^2 = 0.65$ GeV^2, (b) $W = 1.750$ GeV and $-q^2 = 1.55$ GeV^2, (c) $W = 1.875$ GeV and $-q^2 = 0.65$ GeV^2, (d) $W = 1.950$ GeV and $-q^2 = 1.55$ GeV^2, (e) $W = 2.050$ GeV and $-q^2 = 0.65$ GeV^2, and (f) $W = 2.150$ GeV and $-q^2 = 1.55$ GeV^2, where θ and W are the scattering angle and energy in the $K\Lambda$ c.m. frame, and q^2 is the square of the virtual-photon four-momentum. The $-q^2 = 0.65$ GeV^2 results were obtained with $E = 2.567$ GeV and the $-q^2 = 1.55$ GeV^2 results with $E = 4.056$ GeV, where E is the energy of the incident electron in the laboratory frame. Curve identification is as in Fig. 2. Data are from Ref. [27].

were, in turn, input into a new fit of the coupling-strength products, and the whole procedure iterated until convergence of the parameters was obtained.

At each step, we minimized the χ^2 per degree of freedom defined by the relation

$$\nu\chi^2 = \sum \frac{(Y_{\rm calc} - Y_{\rm expt})^2}{\sigma^2}, \tag{45}$$

where the sum is over the data points included in that step, $Y_{\rm calc}$ and $Y_{\rm expt}$ are the calculated and experimental values of the observable, respectively, σ^2 is the squared statistical uncertainty in $Y_{\rm expt}$, and the number of degrees of freedom ν is just the difference between the number of data points included in the sum and the number of parameters included in that step of the iteration procedure. The degree of convergence of the procedure was measured by comparing the χ^2 values obtained in successive iterations. In practice we found that the procedure converges quite well after only two iterations. We also tried varying the starting parameters, but that did not significantly improve the final fit.

V. NUMERICAL RESULTS AND DISCUSSION

Table II lists the coupling-strength parameters obtained in the two fits reported here along with those reported in Ref. [35]. The corresponding values obtained for the electromagnetic form factor parameters are listed in Table III.

A brief examination of the contents of Table II indicates that the coupling strengths obtained in the three fits are quite similar. Among the nucleon resonances, the largest differences occur for the less-well-established resonances of higher mass, where in a couple of cases, there are sign differences between the present fits and the fit of Ref. [35]. There are also some sizable differences for some of the hyperon resonance couplings but, as discussed in Refs. [10,35], the u-channel parameters obtained in fits of electromagnetic strangeness production are highly correlated, so that differences in u-channel parameters obtained in different fits should not be invested with too much significance. In general, the differences between the two fits obtained in this work, both

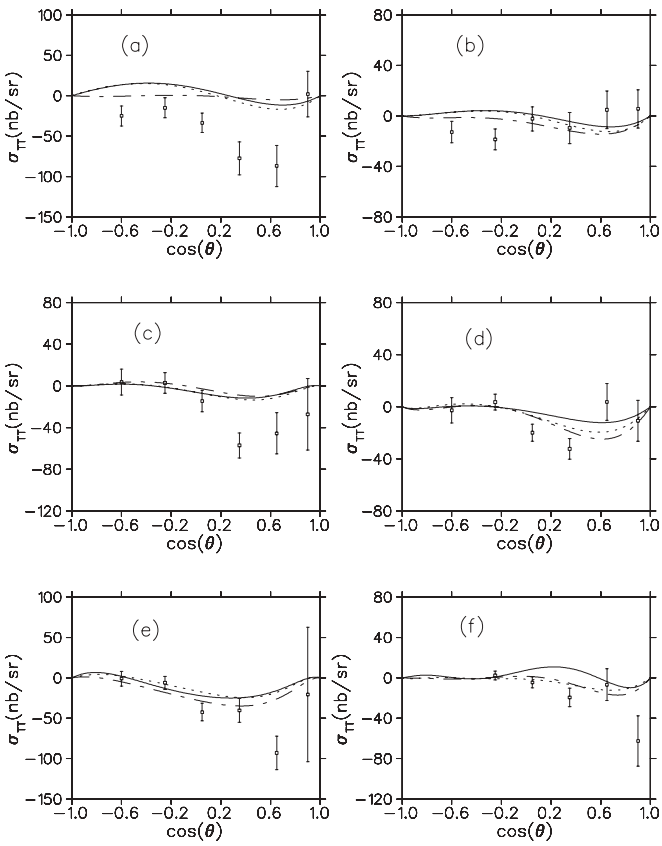

FIG. 10. σ_{TT} vs cos(θ) for the same values of W and $-q^2$ as in Fig. 9, where θ and W are the scattering angle and energy in the $K\Lambda$ c.m. frame, and q^2 is the square of the virtual-photon four-momentum. Curve identification is as in Fig. 2. Data are from Ref. [27].

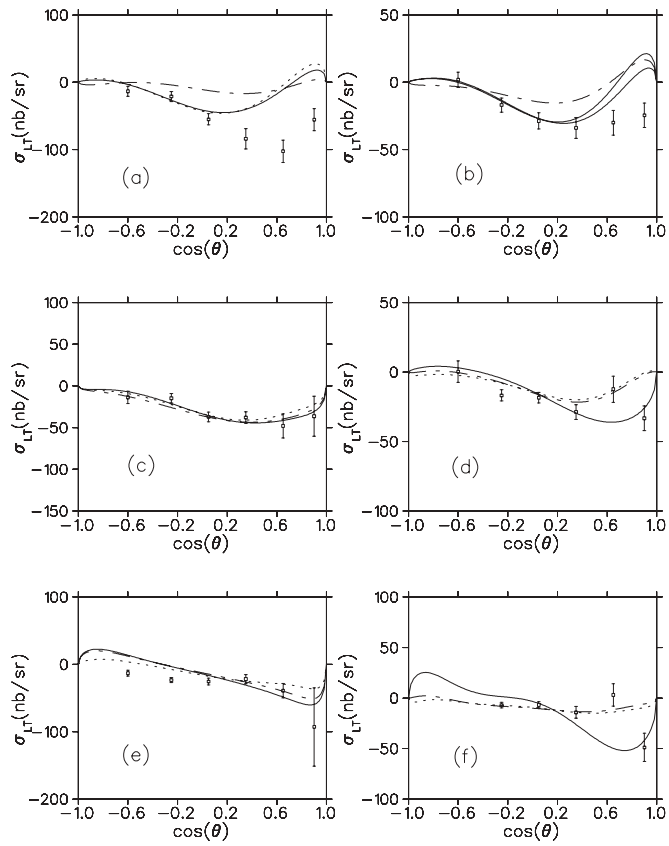

FIG. 11. $\sigma_{LT'}$ vs cos(θ) for the same values of W and $-q^2$ as in Fig. 9, where θ and W are the scattering angle and energy in the $K\Lambda$ c.m. frame, and q^2 is the square of the virtual-photon four-momentum. Curve identification is as in Fig. 2. Data are from Ref. [27].

of which incorporate the $\sigma_{LT'}$ data, are smaller than the differences between either fit and the fit of Ref. [35].

Table III indicates that the form factor parameters obtained in the three fits, like the coupling parameters, are quite similar.

One measure of the relative quality of the three fits is exhibited in Table IV. Here we have tabulated the χ^2 per data point for the photoproduction data alone, for the electroproduction data excluding the $\sigma_{LT'}$ data and for the $\sigma_{LT'}$ data alone for all three fits. We define the χ^2 per data point by Eq. (45), but with the quantity ν on the right-hand side of that equation replaced by just the total number of data points of each type.

A perusal of the values in this table yields several conclusions. All three fits are of comparable quality, which is not surprising given the similarities among the parameter values, but the fits described here are clearly somewhat better than that of Ref. [35]. Comparing the three different data sets, it is obvious that the photoproduction data is fit more successfully than the electroproduction data and that the $\sigma_{LT'}$ is not fit as well as the rest of the electroproduction data. It is interesting that exclusion of the $N(2080)$ and $N(2200)$ resonances slightly reduces the quality of the overall fit, but slightly improves the fit to the $\sigma_{LT'}$ subset of data.

In the remainder of this section, three sets of results are presented. The first set, represented by the dash-dotted curves in each figure, was obtained with the fit of Ref. [35], which did not incorporate the $\sigma_{LT'}$ data. The other two sets were obtained with the fits reported here, which did incorporate the $\sigma_{LT'}$ data. In each figure, the solid curves represent results from the fit with all resonances included, while the dotted curves represent results from the fit with the $N(2080)$ and $N(2200)$ resonances excluded.

The first three figures provide a sampling of our photoproduction results. In Fig. 2 the differential cross section and the hyperon polarization asymmetry P are plotted as functions of cos(θ), the cosine of the c.m. scattering angle, for several values of the c.m. energy W. The two double-polarization observables, C_x and C_z, are shown as functions of cos(θ) in Fig. 3 and the photon beam asymmetry Σ as a function of cos(θ) in Fig. 4.

As the curves in these three figures indicate, the differences in the photoproduction observables obtained in the three fits are quite modest. The largest differences occur at the lowest energy shown, where the fits obtained here seem to yield better descriptions of the data for the hyperon polarization asymmetry P, the photon-beam asymmetry Σ, and the double-polarization observable C_x than the fit of Ref. [35]. The fits also yield somewhat different results for the double-polarization observable C_z at all three energies shown, but none of the fits are clearly superior for this observable. In general, the two fits obtained here yield curves that are closer together than either set of curves is with the curves generated from the

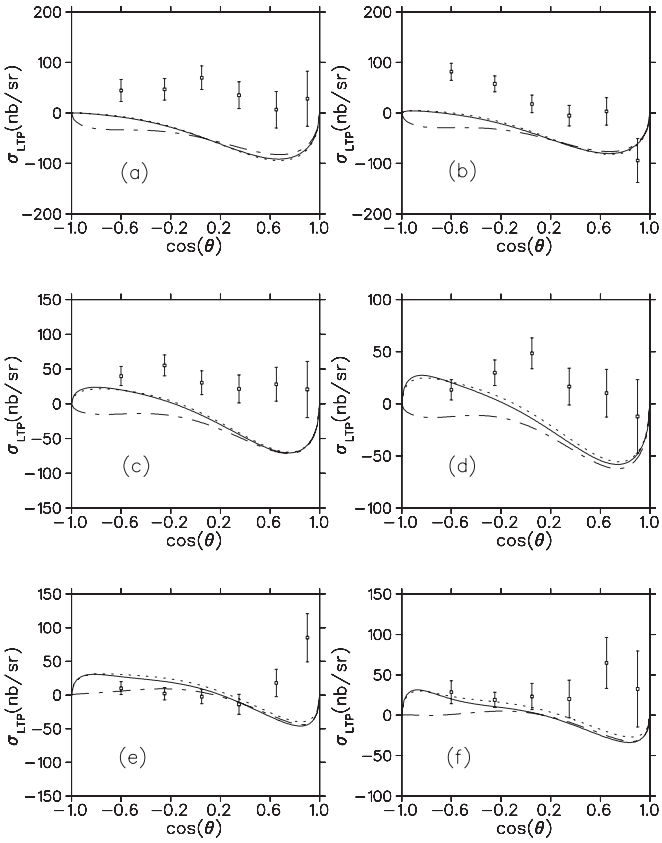

FIG. 12. $\sigma_{LT'}$ vs $\cos(\theta)$ for (a) $W = 1.725$ GeV and $-q^2 = 0.65$ GeV^2, (b) $W = 1.725$ GeV and $-q^2 = 1.00$ GeV^2, (c) $W = 1.825$ GeV and $-q^2 = 0.65$ GeV^2, (d) $W = 1.825$ GeV and $-q^2 = 1.00$ GeV^2, (e) $W = 1.975$ GeV and $-q^2 = 0.65$ GeV^2, and (f) $W = 1.975$ GeV and $-q^2 = 1.00$ GeV^2, where θ and W are the scattering angle and energy in the $K\Lambda$ c.m. frame, and q^2 is the square of the virtual-photon four-momentum. Curve identification is as in Fig. 2. Data are from Ref. [28].

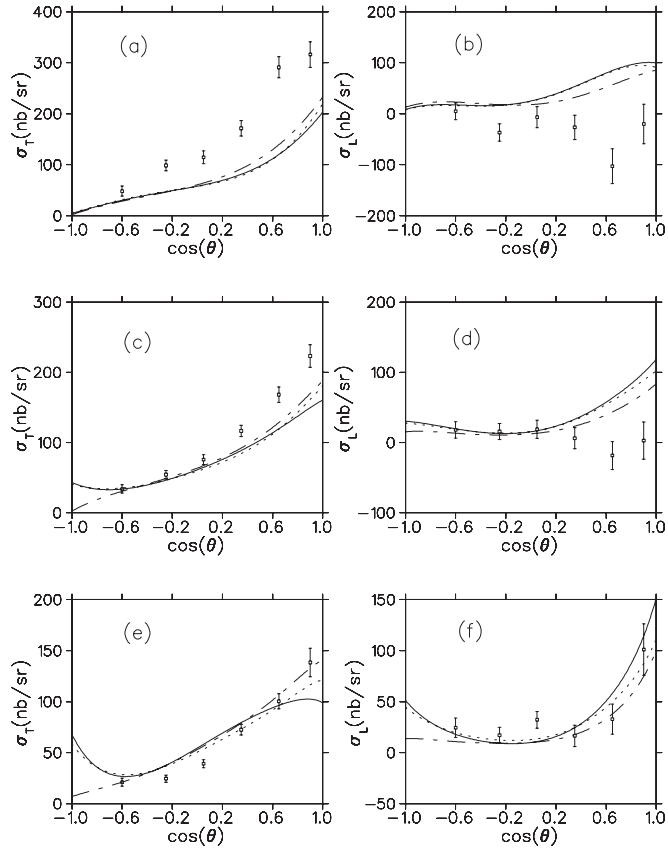

FIG. 13. σ_T vs $\cos(\theta)$ (left-side panels) and σ_L vs $\cos(\theta)$ (right-side panels) for $-q^2 = 1.0$ GeV^2 and $W = 1.750$ GeV [panels (a) and (b)], $W = 1.850$ GeV [panels (c) and (d)], and $W = 1.950$ GeV [panels (e) and (f)], where θ and W are the scattering angle and energy in the $K\Lambda$ c.m. frame, and q^2 is the square of the virtual-photon four-momentum. Curve identification is as in Fig. 2. Data are from Ref. [27].

fit of Ref. [35]. However, this is not always true, as seen in the higher-energy results for P and the double-polarization observables.

Our results for the virtual photoproduction structure functions in the electroproduction experiment are presented in the remaining figures. Figures 5–8 show the structure functions σ_U, σ_{TT}, σ_{LT}, and $\sigma_{LT'}$ as functions of W for various values of $\cos(\theta)$ and $-q^2$, the negative of the squared virtual four-momentum. In Figs. 9–12, the same structure functions are depicted as functions of $\cos(\theta)$ for various values of W and $-q^2$. Figure 13 shows the structure functions σ_T and σ_L as functions of $\cos(\theta)$ for three different energies and $-q^2 = 1.00$ GeV^2, which is the only value of $-q^2$ for which data exist for these two structure functions.

As for the photoproduction observables, the results obtained for the electroproduction observables in the three fits are quite similar. The main differences occur in the structure functions σ_U and σ_{TT} at the higher $-q^2$ value and larger energies. There are also some differences in the σ_U results at back angles and in the $\sigma_{LT'}$ results at forward angles, especially at the higher $-q^2$ value. The similarities in the $\sigma_{LT'}$ results obtained in the three fits is rather surprising since in the two fits obtained here, the $\sigma_{LT'}$ data was included in the fits, while in the fit of Ref. [35] it was not. This seems to indicate that a single quantitative fit to the unpolarized structure functions and the electron beam asymmetry structure function is difficult to achieve in this model.

It is worth noting that, in contrast with the unpolarized structure functions, $\sigma_{LT'}$ involves the imaginary part of a product of two hadronic current components. Because there is just one phase associated with all the components of the hadronic current for a given resonance, the product of any two current components for a single resonance is a real quantity. Hence, the structure function $\sigma_{LT'}$ arises entirely from interferences between different resonances or between resonance and Born contributions. To the extent that there are deficiencies in an effective Lagrangian representation of the Born terms, these deficiencies will manifest themselves most prominently in $\sigma_{LT'}$.

In contrast with the photoproduction results, there are a few instances where the electroproduction results generated with the two fits reported here are rather different. In fact, for some of the structure functions, the fit that excludes the $N(2080)$

and $N(2200)$ resonances yields results that are closer to those obtained with the fit of Ref. [35], especially at the higher $-q^2$ value and larger energies.

Due to the similarities among the three fits, most of the discussion in Ref. [35] regarding the quality of the fit reported there applies equally well here. In general, the fit to the data is best for the structure function σ_U. As seen in Fig. 9, the angular distributions for this structure function reproduce the data at least semiquantitatively. The energy dependence of the σ_U data is not as well reproduced with significant discrepancies between 1.72 and 1.85 GeV at the lower $-q^2$ value and for energies above 2.22 GeV at the higher $-q^2$ value.

The fits to the other structure functions are of generally lower quality than the fit to σ_U. For both σ_{TT} and σ_{LT}, the fits are better at the higher $-q^2$ value. At the lower $-q^2$ value, the fits fail to yield the observed energy dependencies and the observed dip in the angular distribution of σ_{TT} at forward angles is not reproduced.

The model has the most difficulty reproducing the $\sigma_{LT'}$ data. For this structure function, the energy dependence given by the fit is not correct at either $-q^2$ value, and at the two lower-energy values, the calculated angular distributions lie below the data.

In summary, we have updated a previous fit of recent kaon photoproduction and electroproduction data that was based on an effective Lagrangian model supplemented with electromagnetic form factors. We have presented three sets of results, one set obtained with the original fit that did not include the CLAS data for the electron beam asymmetry structure function and the other two obtained with fits that do incorporate that extra data. The three fits yield similar results over most the kinematic range considered, even for the virtual photoproduction structure function $\sigma_{LT'}$ which was included in the fitted data in two of the fits but not in the third.

In addition to the structure functions defined by Eq. (9), there also exist CLAS data for other structure functions related to the polarization of the outgoing Λ hyperon with either an unpolarized or polarized incident electron [29]. The low count rates associated with these structure functions required the use of rather wide kinematical bins, so that comparisons with model calculations or fits employing these data will necessitate the performance of cross-section–weighted averages. Investigations in this direction are currently in progress.

[1] R. A. Adelseck, C. Bennhold, and L. E. Wright, Phys. Rev. C **32**, 1681 (1985); R. A. Adelseck and L. E. Wright, *ibid.* **38**, 1965 (1988); R. A. Adelseck and B. Saghai, *ibid.* **42**, 108 (1990).

[2] Robert A. Williams, Chueng-Ryon Ji, and Stephen R. Cotanch, Phys. Rev. C **46**, 1617 (1992).

[3] T. Mart, C. Bennhold, and C. E. Hyde-Wright, Phys. Rev. C **51**, R1074 (1995); H. Haberzettl, C. Bennhold, T. Mart, and T. Feuster, *ibid.* **58**, R40 (1998); T. Mart and C. Bennhold, *ibid.* **61**, 012201(R) (1999); H. Haberzettl, C. Bennhold, and T. Mart, ACTA Phys. Pol. B **31**, 2387 (2000); Nucl. Phys. A **684**, 475c (2001).

[4] M. K. Cheoun, B. S. Han, B. G. Yu, and Il-Tong Cheon, Phys. Rev. C **54**, 1811 (1996); Bong Son Han, Myung Ki Cheoun, K. S. Kim, and Il-Tong Cheon, Nucl. Phys. A **691**, 713 (2001).

[5] J. C. David, C. Fayard, G. H. Lamot, and B. Saghai, Phys. Rev. C **53**, 2613 (1996); T. Mizutani, C. Fayard, G.-H. Lamot, and B. Saghai, *ibid.* **58**, 75 (1998).

[6] S. S. Hsiao, D. H. Lu, and Shin Nan Yang, Phys. Rev. C **61**, 068201 (2000).

[7] Wen Tai Chiang, F. Tabakin, T.-S. H. Lee, and B. Saghai, Phys. Lett. B **517**, 101 (2001).

[8] Stijn Janssen, Jan Ryckebusch, Wim Van Nespen, Dimitri Debruyne, and Tim Van Cauteren, Eur. Phys. J. A **11**, 105 (2001); Stijn Janssen, Jan Ryckebusch, Dimitri Debruyne, and Tim Van Cauteren, Phys. Rev. C **65**, 015201 (2001); **66**, 035202 (2002); S. Janssen, D. G. Ireland, and J. Ryckebusch, Phys. Lett. B **562**, 51 (2003); S. Janssen, J. Ryckebusch, and T. Van Cauteren, Phys. Rev. C **67**, 052201(R) (2003).

[9] Oren V. Maxwell, Phys. Rev. C **69**, 034605 (2004); **70**, 044612 (2004); **76**, 014621 (2007).

[10] Alejandro de la Puente, Oren V. Maxwell, and Brian A. Raue, Phys. Rev. C **80**, 065205 (2009).

[11] A. Usov and O. Scholten, Phys. Rev. C **72**, 025205 (2005).

[12] A. V. Sarantsev, V. A. Nikonov, A. V. Anisovich, E. Klempt, and U. Thoma, Eur. Phys. J. A **25**, 441 (2005); A. V. Anisovich, V. Kleber, E. Klempt, V. A. Nikonov, A. V. Sarantsev, and U. Thoma, *ibid.* **34**, 243 (2007); V. A. Nikonov, A. V. Anisovich, E. Klempt, A. V. Sarantsev, and U. Thoma, Phys. Lett. B **662**, 245 (2008).

[13] N. Kaiser, T. Waas, and W. Weise, Nucl. Phys. A **612**, 297 (1997).

[14] T. Feuster and U. Mosel, Phys. Rev. C **59**, 460 (1999).

[15] B. Julia-Diaz, B. Saghai, T. S. H. Lee, and F. Tabakin, Phys. Rev. C **73**, 055204 (2006).

[16] B. Borasoy, E. Marco, and S. Wetzel, Phys. Rev. C **66**, 055208 (2002); B. Borasoy, P. C. Bruns, U.-G. Meissner, and R. Nissler, *ibid.* **72**, 065201 (2005); Eur. Phys. J. A **34**, 161 (2007).

[17] M. Q. Tran *et al.*, Phys. Lett. B **445**, 20 (1998); S. Goers *et al.*, *ibid.* **464**, 331 (1999); K. H. Glander *et al.*, Eur. Phys. J. A **19**, 251 (2004).

[18] R. G. T. Zegers *et al.*, Phys. Rev. Lett. **91**, 092001 (2003); M. Sumihama *et al.*, Phys. Rev. C **73**, 035214 (2006).

[19] A. Lleres *et al.*, Eur. Phys. J. A **31**, 79 (2007); A. D'Angelo *et al.*, *ibid.* **31**, 441 (2007).

[20] A. Lleres *et al.*, Eur. Phys. J. A **39**, 149 (2009).

[21] J. W. C. McNabb *et al.*, Phys. Rev. C **69**, 042201 (2004).

[22] D. S. Carman *et al.*, Phys. Rev. Lett. **90**, 131804 (2003); Phys. Rev. C **79**, 065205 (2009).

[23] R. Bradford *et al.*, Phys. Rev. C **73**, 035202 (2006).

[24] R. Bradford *et al.*, Phys. Rev. C **75**, 035205 (2007).

[25] G. Niculescu *et al.*, Phys. Rev. Lett. **81**, 1805 (1998); L. Teodorescu *et al.*, Nucl. Phys. A **658**, 362 (1999); R. M. Mohring *et al.*, Phys. Rev. C **67**, 055205 (2003).

[26] D. S. Carman *et al.*, Phys. Rev. Lett. **90**, 131804 (2003).

[27] P. Ambrozewicz *et al.*, Phys. Rev. C **75**, 045203 (2007).

[28] R. Nasseripour *et al.*, Phys. Rev. C **77**, 065208 (2008).

[29] D. S. Carman *et al.*, Phys. Rev. C **79**, 065205 (2009).

[30] N. Levy, W. Majerotto, and B. J. Read, Nucl. Phys. B **55**, 493 (1973); **55**, 513 (1973); A. Bartl and W. Majerotto, *ibid.* **90**, 285 (1975).

[31] T. Mart and C. Bennhold, Nucl. Phys. A **639**, 237c (1998).
[32] Oren V. Maxwell, Phys. Rev. C **76**, 014621 (2007).
[33] M. Vanderhaeghen, M. Guidal, and J.-M. Laget, Phys. Rev. C **57**, 1454 (1998); M. Guidal, J.-M. Laget, and M. Vanderhaeghen, *ibid.* **61**, 025204 (2000); **68**, 058201 (2003).
[34] B. Golli and S. Sirca, Eur. Phys. J. A **47**, 61 (2011).
[35] Oren V. Maxwell, Phys. Rev. C **85**, 034611 (2012).
[36] J. Beringer *et al.*, Phys. Rev. D **86**, 010001 (2012).
[37] M. Gari and W. Krümpelmann, Z. Phys. A: At. Nucl. **322**, 689 (1985); Phys. Lett. B **173**, 10 (1986); Phys. Rev. D **45**, 1817 (1992).
[38] F. Cardarelli, I. L. Grach, I. M. Narodetskii, E. Pace, G. Salme, and S. Simula, Phys. Rev. D **53**, 6682 (1996).